

Investigation of Feshbach resonances in ultracold ^{40}K spin mixtures

J. S. Krauser,^{1,2} J. Heinze,^{1,2} S. Götze,¹ M. Langbecker,^{1,3} N. Fläschner,¹ L. Cook,⁴ T. M. Hanna,⁵ E. Tiesinga,⁵ K. Sengstock,^{1,2,*} and C. Becker^{1,2,*}

¹*Institut für Laser-Physik, Universität Hamburg, Luruper Chaussee 149, 22761 Hamburg, Germany*

²*Zentrum für Optische Quantentechnologien, Universität Hamburg, Luruper Chaussee 149, 22761 Hamburg, Germany*

³*Institut für Physik, Johannes Gutenberg Universität Mainz, Staudingerweg 7, 55128 Mainz, Germany*

⁴*Department of Physics and Astronomy, University College London, Gower Street, London WC1E 6BT, United Kingdom*

⁵*Joint Quantum Institute, National Institute of Standards and Technology and the University of Maryland, Gaithersburg, Maryland 20899, USA*

(Received 9 January 2017; published 3 April 2017)

Magnetically tunable Feshbach resonances are an indispensable tool for experiments with atomic quantum gases. We report on 37 thus far unpublished Feshbach resonances and four further probable Feshbach resonances in spin mixtures of ultracold fermionic ^{40}K with temperatures well below 100 nK. In particular, we locate a broad resonance at $B = 389.7\text{ G}$ with a magnetic width of 26.7 G. Here $1\text{ G} = 10^{-4}\text{ T}$. Furthermore, by exciting low-energy spin waves, we demonstrate a means to precisely determine the zero crossing of the scattering length for this broad Feshbach resonance. Our findings allow for further tunability in experiments with ultracold ^{40}K quantum gases.

DOI: [10.1103/PhysRevA.95.042701](https://doi.org/10.1103/PhysRevA.95.042701)

I. INTRODUCTION

Ultracold fermionic atomic gases are ideally suited for the study of many-body quantum phenomena owing to the unrivaled control over experimental parameters such as the spatial geometry of confining potentials and the interaction strength between the atoms. The interaction strength is controlled using magnetically tunable Feshbach resonance and typically characterized by the s -wave scattering length, which can be set to a wide range of values, either negative or positive. Feshbach resonances have been found in many bosonic, as well as fermionic, atomic systems (see [1–5] and references therein). The isotope ^{40}K constitutes one of the workhorses in current experiments with ultracold fermions and provides a rich ground-state structure allowing for the realization of binary and multicomponent spin mixtures [6–23], as well as several Bose-Fermi [24–30] and Fermi-Fermi mixtures [31–35]. In the energetically lowest hyperfine manifold with total angular momentum $f = 9/2$ ten magnetic spin states are available ranging from $m = -9/2, \dots, +9/2$, and 45 binary spin mixtures can be realized [36]. So far, only three Feshbach resonances have been reported, one for each of collision channels $\{m_1, m_2\} = \{-9/2, -7/2\}$ [37], $\{-7/2, -7/2\}$ [38,39], and $\{-9/2, -5/2\}$ [40].

Here, we report on the experimental observation of 37 theoretically confirmed and 4 further probable magnetic Feshbach resonances in different spin mixtures of ultracold ^{40}K . Their positions are determined from the enhanced, resonant loss of atoms near the resonance, either caused by three-body recombination or two-body inelastic spin flips. In addition, we introduce a method for precisely determining the sign changes of the scattering length around the Feshbach resonance by exciting low-energy spin waves. In particular, this approach enables us to measure the zero crossing with high accuracy. We also find that the measured positions of the assigned

Feshbach resonances agree well with theoretical calculations based on multichannel coupled-channels and quantum-defect theory using the best available Born-Oppenheimer potentials for ^{40}K [41].

A Feshbach resonance occurs when two atoms in well-defined spin states collide and couple to a virtual molecular state with a different spin configuration [1–5]. Because these configurations have different magnetic moments their relative Zeeman energy can be tuned with a magnetic field. This leads to a magnetic-field-dependent complex scattering length $\tilde{a}(B) = a(B) - ib(B)$, where real-valued $a(B)$ and $b(B) > 0$ describe elastic and inelastic two-body processes, respectively. Here, we have allowed for inelastic transitions to spin configurations whose Zeeman energy is below that of the entrance configuration. In fact, near a resonance and in the limit of zero collision energy,

$$a(B) = a_{\text{bg}} \left[1 - \frac{\Delta B(B - B_{\text{res}})}{(B - B_{\text{res}})^2 + (\gamma_2/2)^2} \right], \quad (1)$$

with resonance position B_{res} , magnetic width ΔB , and background scattering length a_{bg} . Finally, γ_2 describes two-body decay to other spin-channels (expressed in units of the magnetic field). Similarly, we have

$$b(B) = 2a_{\text{res}} \frac{(\gamma_2/2)^2}{(B - B_{\text{res}})^2 + (\gamma_2/2)^2}, \quad (2)$$

with resonance length $a_{\text{res}} = a_{\text{bg}}\Delta B/\gamma_2$. Atom loss, quantified by the two-body rate coefficient $K_2(B) = 4\pi\hbar b(B)/\mu$, is largest in the vicinity of the resonance position B_{res} . Here, \hbar is the reduced Planck constant, $\mu = m/2$, and m is the atomic mass.

II. LOSS SPECTROSCOPY OF FESHBACH RESONANCES

We begin our experiments by preparing a spin mixture of $m_1 = +9/2$ and $m_2 = +7/2$ atoms with about $N = 5 \times 10^4$ atoms per spin state in an optical dipole trap. The trap is harmonic and nearly isotropic with mean trapping frequency

*Corresponding author: cbecker@physnet.uni-hamburg.de

TABLE I. Thirty-seven measured and theoretically assigned Feshbach resonances of ^{40}K and the prediction of a further 17 resonances. The first four columns represent the collision channel $\{m_1, m_2\}$ in the $f = 9/2$ manifold, the total spin quantum number $M = m_1 + m_2$, and the partial wave ℓ , with its projection m_ℓ . The next two columns are the experimental maximum loss position B^{exp} and the observed magnetic width σ^{exp} . The uncertainty of B^{exp} , given in parentheses, is a 1 standard deviation uncertainty with combined systematic and statistical error. The last four columns show resonance data from coupled-channels calculations at a collision energy of $E/k = 60$ nK. Here, $B_{\text{res}}^{\text{calc}}$ is the resonance position, where the elastic rate coefficient K_{elas} has its maximum, ΔB^{calc} is the (signed) magnetic width defined as the difference between the field locations, where K_{elas} has a minimum and maximum, respectively. γ_2 is the two-body decay width, as defined in Eq. (1). Some resonances only exhibit resonant behavior in the calculated losses. We give the corresponding resonance position in the $B_{\text{res}}^{\text{calc}}$ column and mark them with a superscript star. Missing numbers in one or more of the last two columns imply the absence of a minimum in K_{elas} and/or that the collision has no losses. Magnetic fields and widths are in Gauss.

$\{m_1, m_2\}$	M	ℓ	m_ℓ	B^{exp}	σ^{exp}	$B_{\text{res}}^{\text{calc}}$	ΔB^{calc}	γ_2
$\{+5/2, -9/2\}$	-2	s	0	24.0(0.5)	4.2	24.5	2.1	0.24
	-2	s	0			33.2	0.7	1.7
$\{+9/2, -9/2\}$	0	s	0	17.6(0.3)	5.4	18.7	1.8	0.30
	0	s	0	35.9(0.4)	5.6	34.9	4.2	5.1
	0	p	-1	93.6(1.3)	17.3	89.1*		20
	0	p	1	ibid.		88.2		20
	0	p	0	ibid.		98.1	-27.4	21
$\{+7/2, -7/2\}$	0	s	0			18.0	0.2	0.17
	0	s	0	34.3(0.8)	10.8	35.2	3.4	0.77
	0	s	0	65.5(1.3)	11	64.2	7.0	9.1
	0	s	0	147.1(3.0)	0.8	145.8	0.2	0.01
	$\{+9/2, -7/2\}$	1	s	0	13.9(0.2)	1.3	14.4	0.4
1		s	0	28.4(0.3)	6.1	30.2	2.9	0.39
1		s	0	66.3(0.7)	14.5	62.2	11.9	15
1		p	1	139(1)	20	131.6		25
1		p	-1	ibid.		132.5*		25
1		p	0	ibid.		143.0	-41.4	26
$\{+5/2, -5/2\}$		0	s	0			17.6	0.1
	0	s	0	31(4)	6	32.3	0.4	0.38
	0	s	0	61(4)	21	61.6	4.0	1.0
	0	s	0			111.8	0.02	0.001
	0	s	0			156.7	1.0	0.04
$\{+7/2, -5/2\}$	1	s	0			14.2	0.2	0.04
	1	s	0			28.1	0.2	0.22
	1	s	0	61(8)	31	60.0	6.0	0.79
	1	s	0			149.4	0.3	0.13
$\{+9/2, -5/2\}$	2	s	0	27.3(0.3)	4.8	26.8	1.9	1.2
	2	s	0	63.4(0.7)	30	62.1	8.4	6.3
	2	p	1	159(3)	40	157.1		23
	2	p	-1	ibid.		157.1		23
	2	p	0	ibid.		166.1	-46.5	25
$\{+3/2, -3/2\}$	0	s	0			17.4	0.08	0.02
	0	s	0	31(4)	6	31.4	0.2	0.13
	0	p	0	46(4)	4	45.6		0.11
	0	p	1	ibid.		46.4		0.07
	0	p	-1	ibid.		46.4		0.13

TABLE I. (*Continued.*)

$\{m_1, m_2\}$	M	ℓ	m_ℓ	B^{exp}	σ^{exp}	$B_{\text{res}}^{\text{calc}}$	ΔB^{calc}	γ_2	
	0	s	0	53(4)	4	55.3	0.3	0.35	
	0	s	0	95(4)	23	93.6	2.3	1.2	
	0	s	0			98.8*		0.009	
	0	s	0			120.9	0.1	0.0003	
	0	s	0	182(4)	12	181.4	2.3	0.25	
$\{+5/2, -3/2\}$	1	s	0			14.1	0.06	0.007	
	1	s	0	23(8)	8	27.3	0.1	0.04	
	1	s	0	53(8)	8	51.8	0.1	0.07	
	1	s	0			115.4	0.8	0.55	
	1	s	0	122(8)	>40	120.2	7.7	2.5	
	1	s	0			168.8	1.1	0.13	
$\{+9/2, -3/2\}$	3	s	0	53(4)	14	51.9	4.4	2.6	
	3	s	0	137(8)	53	140.4	14.4	5.5	
$\{+1/2, -1/2\}$	0	s	0	15(4)	4	17.3	0.06		
	0	s	0	31(4)	5	30.9	0.2		
	0	s	0	61(8)	8	53.4	0.4		
	0	s	0	88(4)	4	87.1	0.4		
	0	s	0			93.6			
	0	s	0			109.9		0.02	
	0	s	0			145.1		0.03	
	0	s	0	246(0.8)	2.4	246.6		2.0	
$\{+9/2, -1/2\}$	4	s	0	114(8)	>40	112.2	11.7	7.6	
	$\{-1/2, -1/2\}$	-1	p	1	373(2)	2	372.4	30.1	
		-1	p	-1	ibid.		372.4	30.1	0.001
		-1	p	0	ibid.		373.4	-11.5	0.001
		-1	p	1			418.9	8.1	
-1		p	0			418.9	-0.8	0.003	
$\{+3/2, +3/2\}$	3	p	1	140(4)	4	139.6	-37.1		
	3	p	-1	ibid.		139.8	-37.0	0.03	
	3	p	0	ibid.		141.5	-30.5	0.009	

$\bar{\omega} = 2\pi \times 50$ Hz and temperature $T \approx 0.3T_F$, where $T_F = \hbar\bar{\omega}(6N)^{1/3}/k \approx 170$ nK is the Fermi temperature and k is the Boltzmann constant. For the investigation of different collision channels, the corresponding two-component 50:50 spin mixture is prepared at a magnetic field of $B = 45$ G using radio-frequency sweep and pulse protocols optimized for each mixture. After the preparation we do not observe any atoms in undesired spin states within our detection sensitivity of $N_{\text{min}} \approx 200$. After this preparation, the magnetic field is ramped to its final value and the ensemble is held for a time of 100 ms. The magnetic field is calibrated by radio-frequency spectroscopy, resulting in an uncertainty of $\Delta B \leq 0.2$ G. Subsequently, the magnetic field is switched off and the remaining atoms are counted after a time of flight in a Stern-Gerlach gradient field. The field value where atom loss is maximal, B^{exp} , is assigned as the resonance position B_{res} . The full-width-half-maximum magnetic width of the experimental loss feature is denoted by σ^{exp} .

We have located 41 resonant experimental loss features in this manner and assigned 37 based on two complementary

theoretical approaches for collisions between two fermionic ^{40}K atoms. The first approach corresponds to a coupled-channels calculation based on the spectroscopically accurate $X^1\Sigma_g^+$ and $a^3\Sigma_u^+$ Born-Oppenheimer potentials [41] mixed by the atomic Fermi-contact, atomic Zeeman, and magnetic dipole-dipole interactions. The second approach corresponds to a multichannel quantum-defect theory [4,42], where the Born-Oppenheimer potentials are described by their scattering length and common van der Waals dispersion coefficient and mixing is due only to the Fermi-contact and Zeeman interactions. For our ultracold ^{40}K collisions it is sufficient to include collisional channels with $\ell = 0$ or $\ell = 1$ mechanical orbital angular momentum, i.e., s or p partial waves. (Parity reflection symmetry ensures that there is no mixing between even and odd ℓ .)

We find quantitative agreement between the location of experimental loss maxima and theoretical resonance locations obtained from either theory. Table I lists the 37 assigned resonances as well as predictions for 17 additional resonances. The theoretical numbers are those extracted from the coupled-channels calculation at a collision energy of $E/k = 60$ nK. The resonance width ΔB^{calc} is the difference in the magnetic field of the elastic rate coefficient minimum and maximum. For our mainly lossy resonances these two fields correspond to good approximation to a scattering length that is zero and infinite, respectively.

Most of the experimental features are Feshbach resonances with s partial-wave character, while a handful have p -wave character. In fact, for each resonance the partial wave of the incoming collision channel and the corresponding resonant bound state are the same. Interestingly, resonances can overlap within their widths. For example, the experimental loss feature at $B = 122$ G in $\{+5/3, -3/2\}$ collisions are two overlapping s -wave resonances according to our coupled-channels calculations, one at ≈ 115.5 G and one at ≈ 120 G. (We assign the experiment with the latter in the table.) Overlapping p -wave resonances can also occur and correspond to its three rotational projection quantum numbers $m_\ell = \pm 1, 0$. Their degeneracy is lifted only by the magnetic dipole-dipole interaction resulting in B -field splittings that are smaller than our corresponding experimental σ^{exp} , as verified by our coupled-channels calculations. In fact, the lines are not resolved.

The remaining four loss features are probable Feshbach resonances and listed in Table II. For these features we found no corresponding theoretical resonances. Parallel to this work, groups in Munich and Amsterdam have measured other ^{40}K Feshbach resonances in different collision channels [43].

Note that the position of a resonance determined from atom loss measurements contains systematic deviations as reported previously; i.e., $B_{\text{res}} \neq B^{\text{exp}}$ [16]. Similarly, σ^{exp} does not coincide with the calculated γ_2 . Atom loss is not only due to two-body collisions; it is also caused by three-body recombination, where three colliding atoms react to produce a hot molecule. The field-dependent recombination rate coefficient $K_3(B)$, does not need to peak at the same B field or have the same width as $K_2(B)$. In addition, for quantum degenerate Fermi gases of ^{40}K atoms, collective phenomena can modify the resonance feature especially when the scattering length $a(B)$ is large compared to $1/k_F$, where the Fermi wave vector

TABLE II. Four further measured loss resonances in ^{40}K . Columns represent collision channel $\{m_1, m_2\}$ in the $f = 9/2$ manifold, quantum number $M = m_1 + m_2$, the partial wave ℓ , the maximum loss position B^{exp} , and the magnetic width σ^{exp} . For these loss features no corresponding theoretical value exists. Magnetic fields and widths are in Gauss. The partial wave for each resonance has been assigned s wave for equal losses in both components and p wave if losses occur in only one component.

$\{m_1, m_2\}$	M	ℓ	B^{exp}	σ^{exp}
$\{+9/2, -1/2\}$	4	s	61(8)	9
$\{+3/2, +3/2\}$	3	p	76(4)	4
$\{+7/2, +7/2\}$	7	p	105(3)	11
	7	p	182(2)	12

k_F is defined by $\hbar^2 k_F^2 / (2m) = kT_F$ [44]. Finally, line shapes can also be distorted when a large fraction of the atoms is lost.

The collision channel $\{+1/2, -1/2\}$ is of particular interest. It is the magnetic ground state of the spin subspace with zero magnetization $M = m_1 + m_2 = 0$ and, hence, losses due to inelastic two-body collisions can occur only by spin-relaxation from the weak magnetic dipole-dipole interactions [23]. In this mixture, we have located a Feshbach resonance at $B_{\text{res}}^{\text{calc}} = 389.7$ G with a width of $\Delta B^{\text{calc}} = 26.7$ G, which is about three times larger than the width of the commonly used Feshbach resonances in the channels $\{-9/2, -7/2\}$ and $\{-9/2, -5/2\}$.

III. PRECISION DETERMINATION OF FESHBACH RESONANCE PARAMETERS VIA SPIN WAVE ANALYSIS

From an experimental point of view, a broad resonance is desirable as it lowers the technical demands for setting a stable value of the interaction strength close to resonance. Hence, the accurate determination of the resonance position B_{res} and the zero crossing, where $a(B)$ has a node as a function of B , are of particular importance. The latter occurs when $B_{\text{zero}} = B_{\text{res}} + \Delta B$, as can be seen from Eq. (1) when $\gamma_2 \rightarrow 0$. At this zero crossing atom loss tends to be small. Recently, detection methods such as radio-frequency spectroscopy [7,45], collective excitations [46,47], Bloch oscillations [48], and spin segregation [49] have been used to determine the resonance position or the zero crossing. Here, we report on a method based on creating spin-wave excitations near a Feshbach resonance. These excitations are sensitive to the sign of the scattering length $a(B)$ [50] and, in particular, the phase of the spin-wave changes sign as the sign of $a(B)$ changes. Spin waves are an interaction-induced phenomenon and cannot be excited at the zero crossing. For strong interactions close to the pole in $a(B)$, where the sign of $a(B)$ also changes, many-body effects induce additional corrections [44]. Therefore, spin waves are particularly suited for finding the zero crossing of Feshbach resonances.

We excite spin waves with spatially dependent magnetic fields that induce spatially dependent relative phase evolution between the two spin components (for details, see [21]). For this purpose, we first prepare a single-component Fermi gas in spin state $m = +1/2$ in an elongated dipole trap with trapping frequencies $\omega = 2\pi \times (70, 70, 12)$ Hz along the three independent spatial directions. At a magnetic field near the

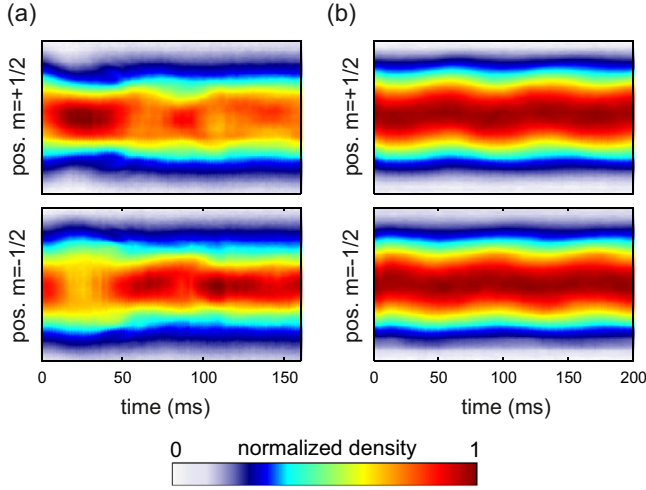


FIG. 1. Breathing and dipole mode resulting from a quadrupole and linear spin wave. Time evolution of the density of the spin components $m = +1/2$ (top row) and $m = -1/2$ (bottom row), obtained by integrating over the two spatial directions orthogonal to the spin-wave excitation. Panel (a) shows quadrupole oscillations induced at $B = 401$ G for strong interactions, and panel (b) shows dipole oscillations induced at $B = 422$ G for weak interactions. Counterflow dynamics between the spin components can be observed in both panels.

$\{+1/2, -1/2\}$ Feshbach resonance at $B_{\text{res}}^{\text{calc}} = 389.7$ G, we subsequently apply a radio-frequency pulse with a duration of $10 \mu\text{s}$ to create a coherent and equal superposition of the spin states $m = +1/2$ and $-1/2$. We then excite a spin wave by using one of two types of field inhomogeneities along the weakest trapping direction. Close to the zero crossing, where the interaction strength is small, we apply a linear magnetic gradient and excite linear spin waves leading to dipole oscillations. For larger interaction strengths small field inhomogeneities are sufficient. Here, even the small residual magnetic quadrupole component originating from the Helmholtz coils excite quadrupole spin waves and spatial breathing modes. Examples of the spatial breathing and dipole modes are shown in Figs. 1(a) and 1(b). In both cases counterflow spin currents between the two spin components are induced, even though the overall density remains constant. While the dipole mode induced near the zero crossing of the resonance is long lived [21], the breathing mode quickly decays due to incoherent collisions in the vicinity of B_{res} [19].

The initial phase and amplitude of the breathing and dipole oscillation depends on the magnetic-field strength. To extract this behavior from our data we analyze the time dependence of the variance of the spatial density profile along the weak trapping direction for the breathing mode and of the displacement of each of the spin components for the dipole mode. The time evolution of the difference in the variance of the two spin clouds is shown in Fig. 2(a) for two magnetic fields on either side of the $B_{\text{res}} = 389.7$ G resonance position. Initially, the differential width grows up to a maximum value and then slowly decays to zero, indicative of strongly damped motion. Figure 2(b) depicts the time evolution of the difference in the displacement of the two spin components for two

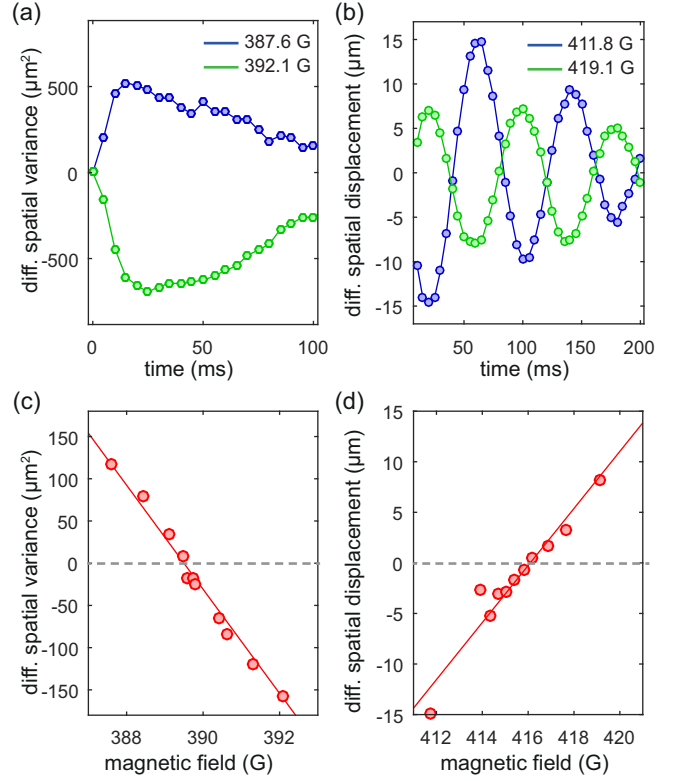


FIG. 2. Spin waves for different magnetic fields. (a) Time evolution of the differential variance for a breathing-mode spin wave at two magnetic fields close to the broad $\{+1/2, -1/2\}$ Feshbach resonance. (b) Time evolution of the differential displacement for a dipole-mode spin wave at two magnetic fields close to the zero crossing of this same resonance. In (a) and (b) the solid lines are only guides to the eye. (c) Maximum amplitude of the differential variance as a function of magnetic field around the resonance position. (d) Amplitude of the differential displacement as a function of magnetic field near the zero crossing. The amplitude is extracted by fitting a damped sine oscillation to data similar to that in panel (b). The positions of the sign change of the scattering length are determined from a linear fit.

magnetic fields on either side of the zero crossing. The dipole oscillations remain visible over several periods. We repeat measurements as shown in Figs. 2(a) and 2(b) for various magnetic fields and find that the observed amplitudes reveal a strong magnetic-field dependence. Figures 2(c) and 2(d) summarize this dependence as a function of magnetic field. Using a linear fit, we can accurately determine the magnetic field at which the spin waves change their oscillation phase. This yields $B_{\text{sw}}^{\text{res}} = 389.5(0.1)$ G and $B_{\text{sw}}^{\text{zero}} = 416.1(0.1)$ G, respectively. The quoted 1 standard deviation uncertainty follows from the fit. We estimate a systematic error due to an uncertainty in the magnetic-field calibration of $\Delta B_{\text{sys}} = 0.2$ G.

The measured value $B_{\text{sw}}^{\text{zero}} = 416.1(0.1)$ G should coincide with the zero crossing of the scattering length. In fact, our measured value is in very good agreement with the theoretical value of 416.4 G. In contrast, the field value $B_{\text{sw}}^{\text{res}}$ is affected by many-body effects and does not serve as a precise measure for the Feshbach resonance position. In future experiments, this could be overcome by using thermal gases, where these effects are negligible [44].

IV. CONCLUSION

In conclusion, we have observed 37 Feshbach resonances in ^{40}K over a broad range of magnetic-field values, as well as four further loss resonances whose origin has not yet been theoretically determined. Thirty-one of the theoretically confirmed resonances have s -wave character and six are p -wave resonances. Most of these resonances are accompanied by losses. In fact, these losses as well as the elastic interactions can be tuned for each Feshbach resonance. This allows for various future applications, such as the study of a quantum Zeno insulator in optical lattices [51,52]. Furthermore, a broad Feshbach resonance in the collision channel $\{+1/2, -1/2\}$ has been identified at a magnetic field of $B = 389.7$ G with a width of 26.7 G, which constitutes an ideal candidate for two-component studies with accurate control over the interaction

strength. In addition, we demonstrated the creation of spin waves around this Feshbach resonance, which allowed for a precise determination of the zero crossing. Furthermore, we observed a phase shift of the spin waves near the Feshbach resonance position, which might allow for the study of many-body effects in strongly interacting Fermi gases in the future.

ACKNOWLEDGMENTS

We acknowledge financial support by the Deutsche Forschungsgemeinschaft (DFG) via Grant No. FOR801 and DFG Excellence Cluster CUI: The Hamburg Centre for Ultrafast Imaging, Structure, Dynamics, and Control of Matter on the Atomic Scale. T.M.H. and L.C. acknowledge support from AFOSR MURI Grant No. FA9550-09-1-0617.

-
- [1] E. Timmermans, P. Tommasini, M. Hussein, and A. Kerman, Feshbach resonances in atomic Bose-Einstein condensates, *Phys. Rep.* **315**, 199 (1999).
- [2] R. A. Duine and H. T. C. Stoof, Atom-molecule coherence in Bose gases, *Phys. Rep.* **396**, 115 (2004).
- [3] T. Köhler, K. Góral, and P. S. Julienne, Production of cold molecules via magnetically tunable Feshbach resonances, *Rev. Mod. Phys.* **78**, 1311 (2006).
- [4] C. Chin, R. Grimm, P. Julienne, and E. Tiesinga, Feshbach resonances in ultracold gases, *Rev. Mod. Phys.* **82**, 1225 (2010).
- [5] C. Chin, R. Grimm, P. Julienne, and E. Tiesinga, Quantum chaos in ultracold collisions of gas-phase erbium atoms, *Nature (London)* **507**, 475 (2014).
- [6] C. A. Regal, M. Greiner, and D. S. Jin, Observation of Resonance Condensation of Fermionic Atom Pairs, *Phys. Rev. Lett.* **92**, 040403 (2004).
- [7] C. Chin *et al.*, Observation of the pairing gap in a strongly interacting fermi gas, *Science* **305**, 1128 (2004).
- [8] G. B. Partridge, K. E. Strecker, R. I. Kamar, M. W. Jack, and R. G. Hulet, Molecular Probe of Pairing in the BEC-BCS Crossover, *Phys. Rev. Lett.* **95**, 020404 (2005).
- [9] M. W. Zwierlein, J. R. Abo-Shaeer, A. Schirotzek, C. H. Schunck, and W. Ketterle, Vortices and superfluidity in a strongly interacting Fermi gas, *Nature (London)* **435**, 1047 (2005).
- [10] R. Jördens, N. Strohmaier, K. Günter, H. Moritz, and T. Esslinger, A Mott insulator of fermionic atoms in an optical lattice, *Nature (London)* **455**, 204 (2008).
- [11] U. Schneider *et al.*, Metallic and insulating phases of repulsively interacting fermions in a 3D optical lattice, *Science* **322**, 1520 (2008).
- [12] S. Ospelkaus *et al.*, Quantum-state controlled chemical reactions of ultracold potassium-rubidium molecules, *Science* **327**, 853 (2010).
- [13] S. Nascimbène, N. Navon, K. J. Jiang, F. Chevy, and C. Salomon, Exploring the thermodynamics of a universal Fermi gas, *Nature (London)* **463**, 1057 (2010).
- [14] A. Sommer, M. Ku, G. Roati, and M. W. Zwierlein, Universal spin transport in a strongly interacting Fermi gas, *Nature (London)* **472**, 201 (2011).
- [15] G. B. Jo *et al.*, Itinerant ferromagnetism in a fermi gas of ultracold atoms, *Science* **325**, 1521 (2009).
- [16] S. Zhang and T. L. Ho, Atom loss maximum in ultra-cold Fermi gases, *New J. Phys.* **13**, 055003 (2011).
- [17] G. J. Conduit and E. Altman, Effect of three-body loss on itinerant ferromagnetism in an atomic Fermi gas, *Phys. Rev. A* **83**, 043618 (2011).
- [18] D. Pekker, M. Babadi, R. Sensarma, N. Zinner, L. Pollet, M. W. Zwierlein, and E. Demler, Competition between Pairing and Ferromagnetic Instabilities in Ultracold Fermi Gases near Feshbach Resonances, *Phys. Rev. Lett.* **106**, 050402 (2011).
- [19] M. Koschorreck, D. Pertot, E. Vogt, and M. Köhl, Universal spin dynamics in two-dimensional Fermi gases, *Nat. Phys.* **9**, 405 (2013).
- [20] J. S. Krauser *et al.*, Coherent multi-flavour spin dynamics in a fermionic quantum gas, *Nat. Phys.* **8**, 813 (2012).
- [21] J. Heinze *et al.*, Engineering Spin Waves in a High-Spin Ultracold Fermi Gas, *Phys. Rev. Lett.* **110**, 250402 (2013).
- [22] J. S. Krauser *et al.*, Giant spin oscillations in an ultracold fermi sea, *Science* **343**, 157 (2014).
- [23] U. Ebling, J. S. Krauser, N. Flaschner, K. Sengstock, C. Becker, M. Lewenstein, and A. Eckardt, Relaxation Dynamics of an Isolated Large-Spin Fermi Gas Far from Equilibrium, *Phys. Rev. X* **4**, 021011 (2014).
- [24] G. Roati, F. Riboli, G. Modugno, and M. Inguscio, Fermi-Bose Quantum Degenerate ^{40}K - ^{87}Rb Mixture with Attractive Interaction, *Phys. Rev. Lett.* **89**, 150403 (2002).
- [25] J. Goldwin, S. Inouye, M. L. Olsen, B. Newman, B. D. DePaola, and D. S. Jin, Measurement of the interaction strength in a Bose-Fermi mixture with ^{87}Rb and ^{40}K , *Phys. Rev. A* **70**, 021601(R) (2004).
- [26] C. Ospelkaus, S. Ospelkaus, K. Sengstock, and K. Bongs, Interaction-Driven Dynamics of ^{40}K - ^{87}Rb Fermion-Boson Gas Mixtures in the Large-Particle-Number Limit, *Phys. Rev. Lett.* **96**, 020401 (2006).
- [27] S. Ospelkaus, C. Ospelkaus, L. Humbert, K. Sengstock, and K. Bongs, Tuning of Heteronuclear Interactions in a Degenerate Fermi-Bose Mixture, *Phys. Rev. Lett.* **97**, 120403 (2006).

- [28] K. Günter, T. Stöferle, H. Moritz, M. Köhl, and T. Esslinger, Bose-Fermi Mixtures in a Three-Dimensional Optical Lattice, *Phys. Rev. Lett.* **96**, 180402 (2006).
- [29] T. Best, S. Will, U. Schneider, L. Hackermüller, D. van Oosten, I. Bloch, and D. S. Luhmann, Role of Interactions in ^{87}Rb - ^{40}K Bose-Fermi Mixtures in a 3D Optical Lattice, *Phys. Rev. Lett.* **102**, 030408 (2009).
- [30] J. W. Park, C. H. Wu, I. Santiago, T. G. Tiecke, S. Will, P. Ahmadi, and M. W. Zwierlein, Quantum degenerate Bose-Fermi mixture of chemically different atomic species with widely tunable interactions, *Phys. Rev. A* **85**, 051602(R) (2012).
- [31] M. Taglieber, A.-C. Voigt, T. Aoki, T. W. Hänsch, and K. Dieckmann, Quantum Degenerate Two-Species Fermi-Fermi Mixture Coexisting with a Bose-Einstein Condensate, *Phys. Rev. Lett.* **100**, 010401 (2008).
- [32] E. Wille, F. M. Spiegelhalter, G. Kerner, D. Naik, A. Trenkwalder, G. Hendl, F. Schreck, R. Grimm, T. G. Tiecke, J. T. M. Walraven, S. J. J. M. F. Kokkelmans, E. Tiesinga, and P. S. Julienne, Exploring an Ultracold Fermi-Fermi Mixture: Interspecies Feshbach Resonances and Scattering Properties of ^6Li and ^{40}K , *Phys. Rev. Lett.* **100**, 053201 (2008).
- [33] T. G. Tiecke, M. R. Goosen, A. Ludewig, S. D. Gensemer, S. Kraft, S. J. J. M. F. Kokkelmans, and J. T. M. Walraven, Broad Feshbach Resonance in the ^6Li and ^{40}K Mixture, *Phys. Rev. Lett.* **104**, 053202 (2010).
- [34] L. Costa, J. Brachmann, A. C. Voigt, C. Hahn, M. Taglieber, T. W. Hänsch, and K. Dieckmann, *s*-Wave Interaction in a Two-Species Fermi-Fermi Mixture at a Narrow Feshbach Resonance, *Phys. Rev. Lett.* **105**, 123201 (2010).
- [35] A. Ridinger *et al.*, Photoassociative creation of ultracold heteronuclear $^6\text{Li}^{40}\text{K}^*$ molecules, *Europhys. Lett.* **96**, 33001 (2011).
- [36] Note that 17 of the 45 binary spin mixtures $\{m_1, m_2\}$ in the $f = 9/2$ manifold are stable against rapid losses due to inelastic two-body spin-exchange collisions that conserve $M = m_1 + m_2$ because of either the Pauli exclusion principle or energy conservation. This includes all binary mixtures in spin states with $|m_1 - m_2| = 1$ or 2. Of these 17 spin mixtures only $\{-9/2, -7/2\}$ is also stable against dipolar relaxation.
- [37] T. Loftus, C. A. Regal, C. Ticknor, J. L. Bohn, and D. S. Jin, Resonant Control of Elastic Collisions in an Optically Trapped Fermi Gas of Atoms, *Phys. Rev. Lett.* **88**, 173201 (2002).
- [38] C. A. Regal, C. Ticknor, J. L. Bohn, and D. S. Jin, Tuning *p*-Wave Interactions in an Ultracold Fermi Gas of Atoms, *Phys. Rev. Lett.* **90**, 053201 (2003).
- [39] C. Ticknor, C. A. Regal, D. S. Jin, and J. L. Bohn, Multiplet structure of Feshbach resonances in nonzero partial waves, *Phys. Rev. A* **69**, 042712 (2004).
- [40] C. A. Regal and D. S. Jin, Measurement of Positive and Negative Scattering Lengths in a Fermi Gas of Atoms, *Phys. Rev. Lett.* **90**, 230404 (2003).
- [41] S. Falke, H. Knockel, J. Friebe, M. Riedmann, E. Tiemann, and C. Lisdat, Potassium ground-state scattering parameters and Born-Oppenheimer potentials from molecular spectroscopy, *Phys. Rev. A* **78**, 012503 (2008).
- [42] T. M. Hanna, E. Tiesinga, and P. S. Julienne, Prediction of Feshbach resonances from three input parameters, *Phys. Rev. A* **79**, 040701(R) (2009).
- [43] J. Walraven and I. Bloch (private communication).
- [44] S. Trotzky, S. Beattie, C. Luciuk, S. Smale, A. B. Bardou, T. Enss, E. Taylor, S. Zhang, and J. H. Thywissen, Observation of the Leggett-Rice Effect in a Unitary Fermi Gas, *Phys. Rev. Lett.* **114**, 015301 (2015).
- [45] C. H. Schunck, Y. Shin, A. Schirotzek, and W. Ketterle, Determination of the fermion pair size in a resonantly interacting superfluid, *Nature (London)* **454**, 739 (2008).
- [46] M. Bartenstein, A. Altmeyer, S. Riedl, S. Jochim, C. Chin, J. H. Denschlag, and R. Grimm, Collective Excitations of a Degenerate Gas at the BEC-BCS Crossover, *Phys. Rev. Lett.* **92**, 203201 (2004).
- [47] J. Kinast, S. L. Hemmer, M. E. Gehm, A. Turlapov, and J. E. Thomas, Evidence for Superfluidity in a Resonantly Interacting Fermi Gas, *Phys. Rev. Lett.* **92**, 150402 (2004).
- [48] M. Gustavsson, E. Haller, M. J. Mark, J. G. Danzl, G. Rojas-Kopeinig, and H. C. Nagerl, Control of Interaction-Induced Dephasing of Bloch Oscillations, *Phys. Rev. Lett.* **100**, 080404 (2008).
- [49] X. Du, L. Luo, B. Clancy, and J. E. Thomas, Observation of Anomalous Spin Segregation in a Trapped Fermi Gas, *Phys. Rev. Lett.* **101**, 150401 (2008).
- [50] K. Miyake, W. J. Mullin, and P. C. E. Stamp, Mean-field and spin-rotation phenomena in Fermi systems: The relation between the Leggett-Rice and Lhuillier-Laloë effects, *J. Phys. (Paris)* **46**, 663 (1985).
- [51] N. Syassen *et al.*, Strong dissipation inhibits losses and induces correlations in cold molecular gases, *Science* **320**, 1329 (2008).
- [52] J. J. Garcia-Ripoll *et al.*, Dissipation-induced hard-core boson gas in an optical lattice, *New J. Phys.* **11**, 013053 (2009).